Theoretical investigation of the influence of reaction and diffusion kinetics upon thin-film reactive diffusion

A. Portavoce[1,*] and G. Tréglia[2]
[1]*CNRS, IM2NP, Faculté des Sciences de Saint-Jérôme case 142, 13397 Marseille, France*
[2]*CNRS, CINAM, Campus de Luminy Case 913, 13288 Marseille, France*
(Received 16 February 2012; revised manuscript received 10 May 2012; published 1 June 2012)

Atomistic kinetic Monte Carlo simulations, considering the thermodynamic model of the nonregular solid solution on a rigid fcc lattice and using the first-neighbor atomic pair interaction Ising model, were performed to investigate the influence of reaction and diffusion kinetics on thin-film reactive diffusion with a semi-infinite substrate. The simulations show that compound bulk energies have no effect on the phase sequence of appearance during sequential phase formation. However, a diffusion asymmetry between the elements composing the solid solution has a strong effect on sequential phase formation. Diffusion asymmetry increases the critical thickness of the simultaneous-to-sequential phase formation transition, modifies the phase formation sequence, and controls which phase is the first to form. Asymmetrical diffusion can promote transient phase formation and can prevent some phases of the bulk phase diagram from forming. In addition, it influences the thicknesses of phases and their lifetimes during thin-film reactive diffusion. Consequently, the control of atom diffusion during reactive diffusion, for example, thanks to the controlled introduction of impurities, should allow the phase formation sequence of a given binary system to be modified.

DOI: 10.1103/PhysRevB.85.224101 PACS number(s): 64.60.Bd, 64.60.Cn, 64.70.K−, 64.60.an

I. INTRODUCTION

Solid-state reaction of a film on a substrate is a widely used process to produce surface coatings or structures made of stacked layers. It is considered a reactive diffusion process, since it involves atom diffusion between the film and the substrate, as well as phase formation in the vicinity of the film/substrate interface. Thin-film reactive diffusion is used to produce films of different thicknesses, from several tens of microns to a few nanometers. Protective surface coatings are usually in the micrometric range.[1] In microelectronics, the Salicide process is used to create ohmic contacts on transistor active regions, thanks to the reaction of a metallic film with silicon.[2] In this case, the thickness of the silicide layer is about 10 nm. Usually, reactive diffusion is modeled at the macroscopic scale taking into account bulk diffusion and interface reaction kinetics.[3–7] Despite that this type of model can generally correctly fit some experimental observations, its use seems less appropriate for nanometer-thick film reaction, and its meaning at the atomic scale needs to be addressed, especially since several experimental observations cannot be understood and simulated using these models. For example, nanometer-thick film reaction may occur via the sequential formation of different phases,[8] instead of the simultaneous formation of all the phases of the phase diagram as for thicker films.[9] In macroscopic analytical models based on bulk diffusion and interface reaction, this phenomenon is qualitatively explained by the competition between the diffusion kinetic in the bulk of the initially formed phase, and the reaction kinetic of the subsequent phase.[3–7] However, this type of model is not used to quantitatively reproduce sequential phase formation, especially since it does not consider phase nucleation. At the atomic scale, reactive diffusion involves atomic interdiffusion between the film and the substrate, as well as phase nucleation and growth in a concentration gradient. In a recent work,[10] we used kinetic Monte Carlo (KMC) simulations to investigate thin-film reactive diffusion at the atomic scale. This study showed that the macroscopic reaction term, explaining the linear growth regime of phases versus time (observed experimentally), is related neither to an interface effect nor to a diffusion asymmetry between the film and the substrate. It corresponds to the initial process of phase nucleation and growth without long-range atomic transport in the interdiffusion gradient located at the film/substrate interface. The model used in this study considered a binary solid solution built on a rigid fcc lattice exhibiting a symmetrical phase diagram around the 50% concentration, with the formation of the $L1_0$ and the two $L1_2$ phases. In addition, the two types of atoms had identical diffusion (symmetrical diffusion). In this case, it was shown that the sequential phase formation process results from the formation of an asymmetric interdiffusion profile due to a size effect linked to the finite thickness of the film compared to the substrate thickness (semi-infinite). This symmetrical model (on diffusion and reaction) can reproduce the linear-to-parabolic time-dependence phase growth transition, as well as the thickness-controlled simultaneous-to-sequential phase formation transition, which are both observed experimentally. However, some of the experimental phenomena cannot be reproduced, as the transient phases[11,12] and the missing phases[11] during sequential formation. Consequently, these phenomena could be attributed to asymmetric phase reaction rates or asymmetric diffusion kinetics, as well as a competition between diffusion and reaction kinetics. Furthermore, we suggested[10] that an asymmetric phase diagram, with higher (or lower) phase energies for compounds richer in one of the system elements, as well as asymmetric diffusion, may modify the critical thickness of the simultaneous-to-sequential phase formation transition. These suggestions are supported by previous investigations showing that diffusion asymmetry in a binary solid solution influences both dissolution[13,14] and nucleation.[15]

 ©2012 American Physical Society

Therefore, the goal of the present work is to investigate the influence of reaction rate and diffusion at the atomic scale on reactive diffusion, and their roles on the phase sequence during sequential phase formation. To this aim, the Ising model applied up to the first-neighbor atoms was used to calculate the internal energy of a binary nonregular solid solution build on a rigid fcc lattice. First, this model was used to investigate phase nucleation and atomic diffusion in a composition gradient using a mean-field description. The same model then was used to simulate at the atomic scale, the evolution of the solid solution by KMC. KMC simulations allow us to simulate reactive diffusion of thin films, taking into account the thermodynamic equilibrium driving forces, the atomic transport and ordering kinetics, as well as nucleation, surface segregation, the possible formation of nonordered solid solutions, and phase mixing. In our model (rigid lattice without stress), the nucleation energy depends on the balance between interface energy and bulk energy, and both interface and bulk energies result from atomic pair energies. Thus, interface (and surface) energy depends on composition in the same way as bulk energy. Two cases were considered: (i) a binary solution with asymmetrical phase energies versus composition, without diffusion asymmetry (influence of reaction rate) and (ii) the same solution with diffusion asymmetry (influence of diffusion). Our solid solution contains two types of generic atoms named A and B; however, the thermodynamic and kinetic parameters of the model were fitted on the experimental Si-Ni binary system in order to simulate realistic variations of diffusion and reaction.

The simulations show that compound bulk energies (i.e., reaction rates) have negligible effects on the phase sequence during sequential phase formation. For a system with asymmetric compound energies, the phase sequence is the same as for a symmetric system. Furthermore, despite the large compound energy asymmetry of our system versus composition, the same sequence is observed for the reaction of an A film on a B substrate and of a B film on an A substrate. In contrast, diffusion asymmetry between A and B atoms has a significant impact on the interdiffusion profile and, thus, on the phase sequence. Diffusion asymmetry modifies the order of the phases in the sequence, leading to a different phase sequence order in the case of the reaction of A atoms on a B substrate and of B atoms on an A substrate. In addition, diffusion asymmetry increases the critical thickness of the simultaneous-to-sequential phase formation transition, promotes transient phase formation, and prevents some phases from the equilibrium phase diagram from appearing. Diffusion asymmetry is also shown to influence the phase thicknesses and their lifetimes during reactive diffusion. In consequence, the usual picture of reactive diffusion depicting sequential phase formation as the result of competition between bulk diffusion and interface reaction appears to be inaccurate. KMC simulations show that sequential phase formation results from the formation of an asymmetric interdiffusion profile triggered either by a size effect between the film thickness and the substrate thickness, or by the diffusion competition between the different elements of the system in the bulk of the different compounds.

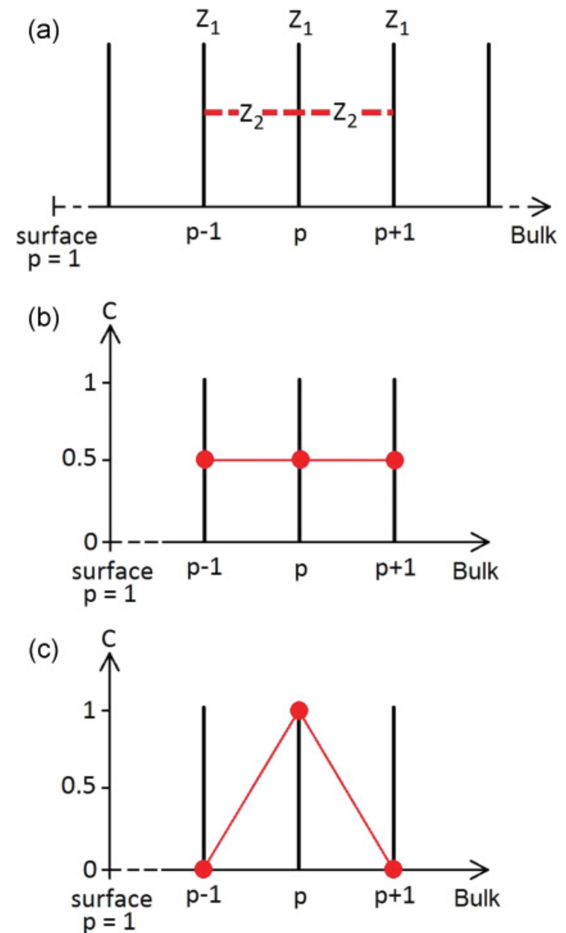

FIG. 1. (Color online) Schematic of the 1D structure [fcc atomic planes in the (001) direction] of the solid solution used for mean-field calculations (a), concentration of A atoms in three consecutive atomic planes of this fcc crystal in case of the 50% random solution (b), and in the case of the $L1_0$ phase (c).

II. MEAN-FIELD CALCULATIONS

A. Crystal energy

The reaction of a thin film on a pure substrate involves atomic redistribution in a strong composition gradient. Therefore, before simulating at the atomic scale the reaction of a film on a substrate, it is interesting to characterize (at least qualitatively) the expected effects of a composition gradient on atom ordering and mobility. To this aim, we chose to use a mean-field description of a general binary solid solution built on an fcc rigid lattice. It is considered that the solution contains two types of generic atoms identified as A atoms and B atoms, with C the global concentration of A atoms in the solution, and $(1 - C)$ the global content of B atoms. Considering a one-dimensional description of the crystal along the (001) direction, the atomic lattice can be described as a succession of (001) atomic planes p containing the same number of atoms N_p, with $p = 1$ at the surface and $p \to \infty$ deeper in the bulk [Fig. 1(a)]. We define C_p as the concentration of A atoms in the plane p, with $(1 - C_p)$ the concentration of B atoms in the same plane. Each atom of the (001) planes in the fcc lattice possesses the same number of first neighbors in the planes (Z_1) and between the planes (Z_2), with $Z_1 = Z_2 =$

$Z = 4$ [Fig. 1(a)]. According to the Ising model, the crystal energy at zero Kelvin (E_{tot}) can be expressed as pairwise interactions between first-neighbor atoms.[16–18] Considering the crystal description presented in Fig. 1(a), the total energy of the A-B solution can be expressed as the sum of the crystal (001) plane energies E_p

$$E_{\text{tot}} = \sum_p E_p, \tag{1}$$

with

$$E_p = \frac{1}{2} N_p Z \left\{ \begin{matrix} \varepsilon^{AA}\left(C_p^2 + C_p C_{p-1} + C_p C_{p+1}\right) \\ +\varepsilon^{BB}[(1-C_p)^2 + (1-C_p)(1-C_{p-1}) + (1-C_p)(1-C_{p+1})] \\ +\varepsilon^{AB}\begin{bmatrix} 2C_p(1-C_p) + C_p(1-C_{p-1}) + C_p(1-C_{p+1}) \\ +(1-C_p)C_{p-1} + (1-C_p)C_{p+1} \end{bmatrix} \end{matrix} \right\}. \tag{2}$$

$\varepsilon^{ij} < 0$ is the first-neighbor i-j atomic pair energy. For example, it is well known that a binary random solution exhibiting ordering tendency with $C = 0.5$ can minimize its internal energy by getting ordered according to the $L1_0$ order.[19] In this case, the random solution for which $C_p = 0.5$ in every atomic plane [Fig. 1(b))], gets ordered following periodical concentration variations between adjacent planes corresponding to $C_p = 1/C_{p+1} = 0$ [Fig. 1(c)]. According to Eq. (2), the energy of each atomic plane in the random solution is $E_p^{\text{rdm}} = 3/8\ N_p Z(\varepsilon^{AA} + \varepsilon^{BB} + 2\varepsilon^{AB})$. The ordered solution contains two types of atomic planes, the planes with $C_p = 1$, for which $E_p^1 = 1/2 N_p Z(\varepsilon^{AA} + 2\varepsilon^{AB})$, and the planes with $C_p = 0$, for which $E_p^2 = 1/2 N_p Z(\varepsilon^{BB} + 2\varepsilon^{AB})$, also from Eq. (2). Consequently, for an infinite crystal (neglecting surface energies), the energy difference between the $L1_0$ phase and the random solution is

$$\Delta E = \left(E_p^1 + E_p^2\right) - 2E_p^{\text{rdm}} = -\tfrac{1}{2} N_p Z V, \tag{3}$$

with

$$V = \tfrac{1}{2}(\varepsilon^{AA} + \varepsilon^{BB} - 2\varepsilon^{AB}). \tag{4}$$

For a system with ordering tendency $V > 0$,[10] leading to $\Delta E < 0$. As expected, the $L1_0$ order allows a reduction of the solid solution energy at a temperature (T) of 0 K.

B. Phase nucleation in a concentration gradient

In order to obtain the $L1_0$ phase from a random 50% A-B solution, a $L1_0$ nucleus needs to form in the random solution. At the beginning of the $L1_0$ nucleus formation, the composition of the nucleus may be nonstoichiometric.[20] In our case it corresponds to composition variations between consecutive atomic planes around the composition $C_p = 0.5$, which will tend over time to the periodic variation $C_p = 1/C_{p+1} = 0$ [Fig. 1(c)]. Figure 2(a) presents the case of the formation of a composition variation between two consecutive atomic planes in a composition gradient. It is considered that this first variation is the formation beginning of the $L1_0$ nucleus, C_p^i is defined as the initial concentration of A atoms in the atomic plane p in the concentration gradient before nucleation, and C_p is defined as the concentration of A atoms in the plane p after nucleation. $\Delta C^* = C_3^i - C_2^i$ characterizes the size of the initial concentration gradient [Fig. 2(a)] that is equal to $\Delta C^*/dx$, with dx the distance between atomic plans [Fig. 2(a)]. $\Delta C = C_3 - C_2$ corresponds to the amplitude of the concentration variation between the consecutive planes 2 and 3 in the phase nucleus [Fig. 2(a)]. In order to characterize this concentration variation amplitude, we define dC as $\Delta C = \Delta C^* + dC$, with $-1 \leqslant \Delta C^* \leqslant 0$ and $0 \leqslant dC \leqslant 1 - \Delta C^*$ [Fig. 2(a)]. One can note in Fig. 2(a) that for $1 \leqslant p \leqslant 4$, $C_p^i = C_1 + (p-1)\Delta C^*$, in addition, $C_0^i = C_1 - \Delta C^*$ and $C_5^i = \Delta C^* + 1 + C_1$. Furthermore, $C_0 = C_0^i$, $C_1 = C_1^i$, $C_4 = C_4^i$, and $C_5 = C_5^i$ [Fig. 2(a)]. In our case, we consider that the composition variation in the nucleus is symmetrical, and forms in the center of the concentration gradient around the composition $C = 0.5$, which corresponds to the $L1_0$ stability domain. Considering that $(C_3 - C_2)/dx = \Delta C/dx$, and $C_3 = 1 - C_2$, we obtain $C_2 = 1/2(1 - \Delta C^* - dC)$ and $C_3 = 1/2\ (1 + \Delta C^* + dC)$. Using these last expressions

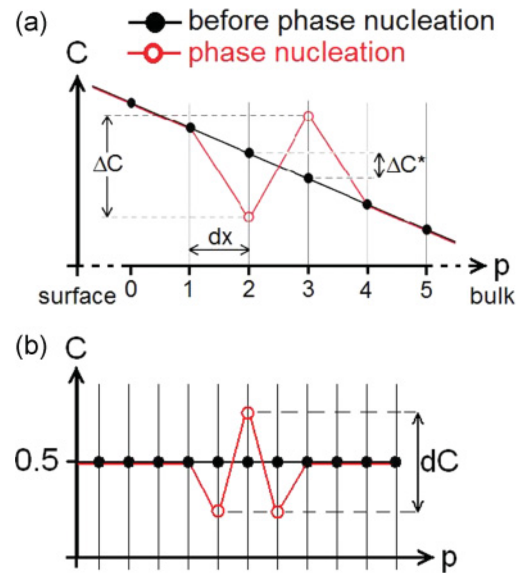

FIG. 2. (Color online) (a) Schematic corresponding to the nucleation of the $L1_0$ phase in a concentration gradient along the (001) atomic planes of the fcc crystal considered for mean-field calculations in case of a two-plane-thick nucleus. (b) Schematic corresponding to the nucleation of the $L1_0$ phase in a 50% random solution on the same fcc crystal in the case of a three-plane-thick nucleus.

and Eqs. (1) and (2), we can show that

$$\Delta E_{\text{tot}} = 3N_p Z \Delta C^* dCV, \quad (5)$$

with ΔE_{tot} the energy difference between the final state after nucleation (composition variations around $C_p = 0.5$), and the initial state before nucleation (composition gradient). By definition $\Delta C^* \leqslant 0$ and $dC \geqslant 0$, and in our case $V \geqslant 0$, consequently, $\Delta E_{\text{tot}} \leqslant 0$: The nucleus formation in the composition gradient allows the system internal energy to be decreased. Equation (5) shows that (i) the larger the compound stability (i.e., the larger the absolute value of V), the larger the energy gain related to the nucleus formation; (ii) the larger the composition difference in the two consecutive planes in the nucleus (i.e., the larger dC), the larger the energy gain allowed by the phase nucleation, which is in agreement with the stability of the $L1_0$ phase compared to the stability of the random solution [Eq. (3)]: The more the composition difference between the planes in the nucleus tends to the plane variation in the $L1_0$ phase [$C_p = 1$ / $C_{p+1} = 0$, Fig. 1(c)], and the stronger the system energy gain; (iii) the stronger the initial composition gradient (i.e., larger is ΔC^*), the larger the energy gain due to nucleation; and (iv) if there is no concentration gradient (i.e., $\Delta C^* = 0$), the nucleus formation does not allow any energy gain. Concerning point (iv), one has to note that our case corresponds to the case of a nucleus made of two consecutive planes only. If the number of atomic planes increases in the nucleus, ΔE_{tot} is not always equal to zero for the random solid solution ($\Delta C^* = 0$). ΔE_{tot} can depend on V, as well as on the atomic pair energies of the pure elements. For example, Fig. 2(b) presents the $L1_0$ nucleation in a random solution with $C_p = 0.5$, with a nucleus made of three atomic planes. In this case, $\Delta C^* = 0$ giving $\Delta C = dC > 0$, and we can show that

$$\Delta E_{\text{tot}} = \frac{3}{4} N_p Z dC \left(\varepsilon^{BB} - \varepsilon^{AA} - \frac{dC}{3} V \right). \quad (6)$$

Thus, $\Delta E_{\text{tot}} < 0$ if $\varepsilon^{BB} - \varepsilon^{AA} < 1/3\ dCV$. Similarly to Eq. (5), in Eq. (6) the parameter V controls the tendency to form ordered phases in the bulk; however, the difference ($\varepsilon^{BB} - \varepsilon^{AA}$) can be interpreted as the term controlling the composition of the two interfaces of the nucleus. Depending on its value, nucleus boundaries rich either in A or in B, will be energetically favored. If $\varepsilon^{BB} = \varepsilon^{AA}$, then $\Delta E_{\text{tot}} = -1/4\ N_p Z\ dC^2\ V < 0$. Equation (5) also shows that if the composition variation in the two consecutive planes of the nucleus is similar to the concentration gradient [$C_3 > C_2$ in Fig. 2(a)], i.e., if the concentration variation in the nucleus increases the gradient concentration, the nucleus increases the system internal energy ($\Delta E_{\text{tot}} > 0$). In summary, a concentration gradient in a binary solid solution with ordering tendency has an important energy cost that favors phase nucleation.

C. Diffusion in a concentration gradient

Using the former definitions used to characterize phase nucleation in a composition gradient, we can show that in the case of a single atom exchange between an atom A in the atomic plane 2, and an atom B in the plane 3 in Fig. 2(a), we have $C_2 = (N_2^i - 1)/N_p$ and $C_3 = (N_3^i + 1)/N_p$, giving $C_2 = C_2^i - 1/N_p$ and $C_3 = C_3^i + 1/N_p$. Thus, for a single atomic exchange we obtain

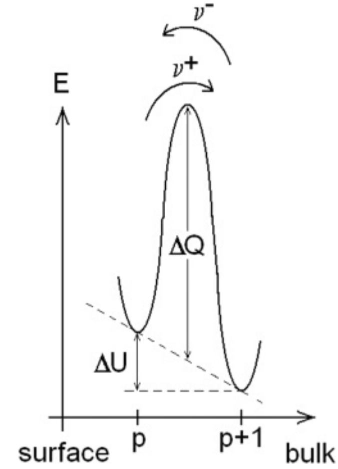

FIG. 3. Classical model used for the description of atomic transport in materials: ΔU is the energy gain of the system after the atomic jump, ΔQ is the diffusion activation energy, and ν^+ and ν^- are the atomic jump frequencies in the $p \rightarrow p+1$ direction and in the $p+1 \rightarrow p$ direction, respectively.

$$\Delta E_{\text{tot}} = 6Z\Delta C^* V. \quad (7)$$

Now, ΔE_{tot} corresponds to the energy gain resulting from an atomic exchange between two consecutive planes in a concentration gradient. Equation (7) also shows that the energy gain is zero if the atomic exchange does not take place in a concentration gradient (i.e., if $\Delta C^* = 0$). This is in agreement with classical Fick's equations that consider the concentration gradient as the diffusion driving force (i.e., the diffusion flux is zero without a concentration gradient). Figure 3 presents a common model often used to model diffusion at the atomic scale. In our case, ΔU corresponds to the energy gain when exchanging an A atom with a B atom from two different consecutive planes in a concentration gradient. ΔQ corresponds to the energetic barrier for diffusion. ν^+ and ν^- are the exchange frequencies toward or against the concentration gradient, respectively. According to this model, the total exchange frequency Γ thus can be expressed as

$$\Gamma = \nu^+ - \nu^- = 2\nu_0 \exp\left(-\frac{Q}{k_B T}\right) \sinh\left(\frac{|6Z\Delta C^* V|}{2k_B T}\right), \quad (8)$$

with k_B the Boltzmann constant. This equation shows that in a concentration gradient (i) the stronger the concentration gradient (i.e., the larger ΔC^*), the larger the atomic exchange frequency, and (ii) the larger the compound stability (i.e., larger is the absolute value of V), the larger the exchange frequency. Consequently, mean-field calculations show that when a concentration gradient is formed between two pure elements with ordering tendency, two mechanisms can take place simultaneously aiming to reduce the energy cost of the concentration gradient: (i) long-range atomic transport (diffusion) allowing for an energy reduction by decreasing the concentration gradient and (ii) phase nucleation (and growth) allowing for an energy decrease without long-range atomic transport, thanks to local new atomic organization (order). The stronger the concentration gradient and the larger the

phase enthalpy, the stronger the driving forces for both atomic diffusion and phase nucleation.

III. ATOMISTIC MONTE CARLO SIMULATIONS

A. Crystal energy

In order to model the effect of the influence of compound energies (i.e., reaction rate) on the simultaneous-sequential phase formation transition, and on the phase sequence during sequential phase growth, one can study thin film reaction in the case of a binary system with asymmetric compound energy versus composition. Our goal was to define such a system, keeping a simple physical relationship with our previous study concerning symmetric systems,[10] in order to perform reasonable comparisons between symmetric and asymmetric cases and to draw general conclusions. To do so, we decided to consider the same first-neighbor pairwise atomic interactions model, the same fcc rigid lattice, and the same type of atomic exchanges using the Metropolis algorithm as previously done in Ref. 10. However, we considered a binary A-B atoms system exhibiting a parameter V varying with concentration.[21] In order to ensure a constant V for every given atomic exchange in the forward and backward directions, we chose to express the V composition variation versus a local concentration C^*. For a given A-B atom pair on the fcc lattice, C^* was calculated taking into account the two considered A and B atoms, their first neighbors, and the first neighbors of the latter. One can note that, in our case, for a given atomic exchange, only the energy of the two exchanged atoms, as well as the energy of their first neighbors, can change. Furthermore, the local concentration C^* is constant before and after the atomic exchange, which leads to a constant value V for forward and backward exchanges. In order to simulate phenomena (e.g., diffusion, nucleation, and reaction) of realistic magnitude, the parameter $V(C)$ was determined from experimental and theoretical formation energies (ΔH) of the Si-Ni compounds,[22,23] using the relation $\Delta H = N Z_v C(1 - C)V$. N is the total number of atoms in the solution, and Z_v is the number of atom first neighbors in the solution bulk (=12 for a fcc lattice). Figure 4 presents the experimental (solid squares) and theoretical (open squares) Si-Ni compound formation energies versus Si composition (A atoms in our case), as well as the function $V(C)$ (solid line and open circles) versus A composition. ε^{AA} and ε^{BB} being constant in Eq. (4), V composition dependence also can be defined through the parameter $\varepsilon^{AB}(C)$. In order to be as realistic as possible, ε^{AA} and ε^{BB} were determined on the rigid fcc lattice taking into account the difference of surface energy between Si (surface tension: 1250 mJ m^{-2}) and Ni (surface tension: 2450 mJ m^{-2}). To this aim, the bulk atomic densities of Si ($\rho \sim 5.0 \times 10^{22}$ at cm^{-3}) and Ni ($\rho \sim 9.14 \times 10^{22}$ at cm^{-3}) were used to define the energy scale of pure element atomic pair energies A-A and B-B on the fcc lattice, using the cohesive energies of Si ($E_{\rm coh}$ $\sim$ 4.63 eV at^{-1}) and Ni ($E_{\rm coh} \sim$ 4.44 eV at^{-1})[24], as well as the atomic volume Ω ($\sim$1.09 $\times$ 10^{-23} cm^3) of the Ni fcc lattice. For Si $E_{\rm coh} \times \Omega\rho = -2.52$ eV at^{-1}, and for Ni $E_{\rm coh} \times \Omega\rho = -4.42$ eV at^{-1}. Thus, for the A-B nonregular solid solution on the fcc lattice, we obtained $\varepsilon^{AA} = -2.52/12 = -0.21$ eV at^{-1} and $\varepsilon^{BB} = -4.42/12 = -0.37$ eV at^{-1}. Considering that

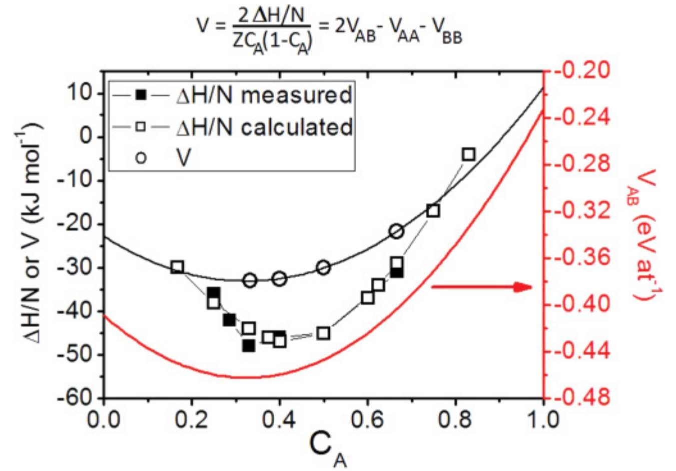

FIG. 4. (Color online) Formation energies of the A-B compounds (left axis, open and solid squares, kJ mol^{-1}), A-B interaction parameter V (left axis, solid line and open circles, kJ mol^{-1}), and the A-B pair energy ε^{AB} (right axis, solid line, eV at^{-1}) versus A concentration ($0 \leqslant C \leqslant 1$).

$V = \Delta H/N \times 1/[Z_v C(C - 1)] = 1/2\,(\varepsilon^{BB} + \varepsilon^{AA} - 2\varepsilon^{AB})$, and using the values of ε^{AA} and ε^{BB}, we defined the function $\varepsilon^{AB}(C)$,

$$\varepsilon^{AB}(C) = -0.409 - 0.328C + 0.505C^2 \text{ eV at}^{-1}. \quad (9)$$

The variation of ε^{AB} versus composition is shown in Fig. 4 (solid line), on the right axis, and the order /disorder phase diagram of our A-B system, calculated by Monte Carlo using the Metropolis algorithm,[25] is presented in Fig. 5. Solid squares correspond to the order /disorder transition critical temperature (T_c) versus composition. Similarly to our previous study,[10] the A-B phase diagram presents three phases: (i) the B-rich $L1_2$ phase (AB_3 compound), (ii) the $L1_0$ phase (AB compound), and (iii) the A-rich $L1_2$ phase (A_3B compound). However, in contrast with the previous case, this phase diagram is not symmetrical around $C = 0.5$. AB_3 is more stable than A_3B, since the formation energy of AB_3 ($T_c \sim 4050\,^\circ$C) is twice the formation energy of A_3B ($T_c \sim 1800\,^\circ$C).

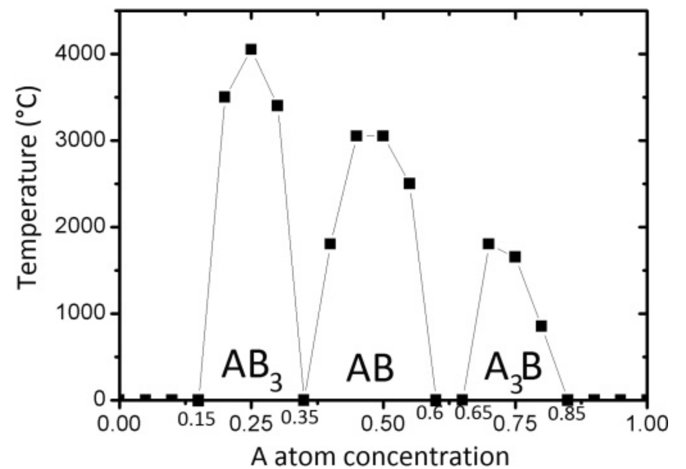

FIG. 5. Order/disorder phase diagram of the A-B nonregular solution characterized by $\varepsilon^{AB} = f(C)$.

B. Monte Carlo kinetics

In order to study the influences of reaction (bulk phase energy) and of diffusion asymmetry independently, two types of KMC simulations were performed. In the first, the system evolution during the reaction of an A (or B, respectively) film on a B (or A, respectively) substrate was simulated using the Metropolis algorithm (M-KMC), in a similar manner to that disclosed in Ref. 10 ($T = 10$ K), in order to allow a direct comparison between the symmetrical and asymmetrical phase diagram cases. Atomic configurations were accepted or rejected depending on internal energy variations calculated using the first-neighbors Ising model. However, in our case, ε^{AB} varies with the local composition C^*, calculated around the considered pair of first-neighbor atoms. Atomic diffusion was simulated thanks to atomic exchanges on the sites of the rigid lattice, the Metropolis algorithm imposing a constant diffusion barrier for all the atomic exchanges (symmetrical diffusion). In this case, the A-B solution bulk energy depended on composition following the phase diagram presented in Fig. 5, but diffusion was independent of composition. These simulations allowed the influence of reaction (phase stability) on reactive diffusion to be studied.

The second type of simulations aimed to consider asymmetric diffusion barriers between pure A and pure B materials, leading to composition-dependent atomic exchange frequency. In order to be coherent with the chosen bulk energy variations with composition, we decided to use the Si-Ni system to define atomic jump frequency variations in the A-B solution versus composition. However, the Ni lattice self-diffusion coefficient [$\sim 1.82\exp(-2.96\,\mathrm{eV}/k_BT)\,\mathrm{cm}^2\,\mathrm{s}^{-1}$][26] is too large compared to the Si coefficient [$\sim 323\exp(-4.705\,\mathrm{eV}/k_BT)\,\mathrm{cm}^2\,\mathrm{s}^{-1}$][27] to be able to simulate diffusion of both elements on a rigid lattice at the temperatures of interest. For example, Ni self-diffusion is five orders of magnitude faster than Si self-diffusion at 1000 °C, and this difference increases as temperature decreases. Nevertheless, the difference of self-diffusion between Si and Ni is lower in grain boundaries (GBs). Ni GB self-diffusion is $\sim 0.08\exp(-1.9\,\mathrm{eV}/k_BT)\,\mathrm{cm}^2\,\mathrm{s}^{-1}$,[28] and Si self-diffusion (Ge diffusion in Si GBs, actually) is $\sim 316.5\exp(-3.34\,\mathrm{eV}/k_BT)\,\mathrm{cm}^2\,\mathrm{s}^{-1}$.[29] Thus, the difference between Si self-diffusion and Ni self-diffusion is only two orders of magnitude at 1000 °C. Consequently, we defined the atomic exchange frequencies in pure A (Γ_A) and pure B (Γ_B) considering GB self-diffusion coefficients in Si and Ni, respectively. One can note that, in experiments, reaction between a film and a substrate (as for Ni silicides) often leads to the formation of polycrystalline layers, and, thus, phase formation during reactive diffusion mainly uses atomic transport through GBs. In the simulations we considered that

$$\Gamma_A = \nu_A \exp\left(\frac{-\Delta E_A}{k_B T}\right) s^{-1} \text{ and } \Gamma_B = \nu_B \exp\left(\frac{-\Delta E_B}{k_B T}\right), \tag{10}$$

with $\Delta E_A = 3.34$ eV, $\Delta E_B = 1.9$ eV, $\nu_A = 4 \times 10^3 \times \nu_0$, $\nu_B = \nu_0$, and $\nu_0 = 10^{13}\ \mathrm{s}^{-1}$ (Debye frequency). Figure 6 presents exchange frequency variations in the pure elements A and B versus temperature. B self-diffusion is faster than A self-diffusion, with a difference of about two orders of magnitude at 1000 °C and of four orders of magnitude at 700 °C. In order

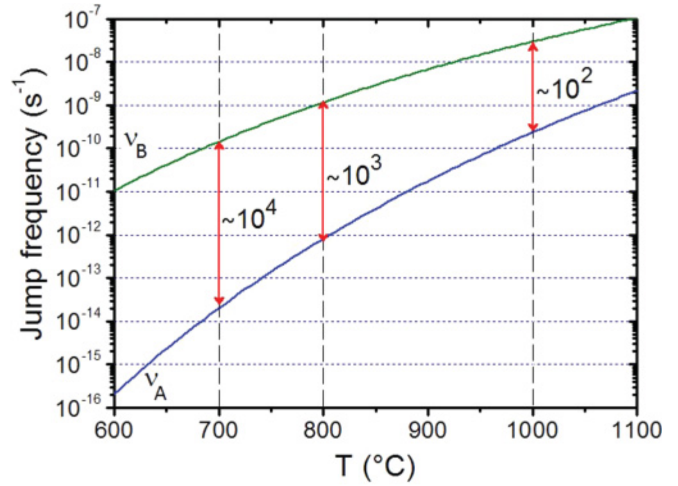

FIG. 6. (Color online) A (Γ_A) and B (Γ_B) atomic jump frequencies versus temperature chosen in the KMC simulations taking into account a diffusion asymmetry between pure A and pure B elements.

to take into account the diffusion asymmetry between A and B in the A-B solution bulk, the atomic exchange frequency variation versus composition was simulated using an atom exchange frequency between first-neighbor atoms on the fcc lattice sites defined as

$$\Gamma = \nu \exp\left(\frac{-\Delta E}{k_B T}\right). \tag{11}$$

Γ was set to depend on the local concentration C^* through two rules of mixtures over ν and ΔE as follows:

$$\Delta E = C^*\Delta E_A + (1 - C^*)\Delta E_B, \tag{12}$$

$$\nu = C^*\nu_A + (1 - C^*)\nu_B. \tag{13}$$

The kinetic evolution of the nonregular A-B solution was simulated using an algorithm similar to the Metropolis one. However, in contrast with previous calculations, in order to take into account the variation of exchange probability versus composition and temperature, the temperature had to be stipulated for these simulations. In this algorithm (noted S-KMC in the text for standard KMC), the variation ΔU of the solution internal energy related to the considered atomic exchange was calculated using Eq. (9) and C^*, as for the previous type of simulations. If $\Delta U < 0$, then the probability of the atomic exchange occurrence was set to

$$Pb = \frac{\nu \exp\left(\frac{-\Delta E}{k_B T}\right)}{2\Gamma_{\max}}. \tag{14}$$

However, if $\Delta U \geqslant 0$, then the probability of the atomic exchange occurrence was set to

$$Pb = \frac{\nu \exp\left(\frac{-(\Delta E + \Delta U)}{k_B T}\right)}{2\Gamma_{\max}}. \tag{15}$$

$\Gamma_{\max}$ is the fastest exchange frequency possible in our A-B system. This way, the occurrence probability of the fastest event was set to 0.5 in the simulations. In our case, $\Gamma_{\max}$ corresponds to B self-diffusion ($\Gamma_{\max} = \Gamma_\mathrm{B}$). According to this model, the atomic diffusion kinetic increases with B

concentration. It is the fastest in a pure B matrix and the slowest in a pure A matrix. This type of simulation allowed the diffusion influence on the reactive diffusion process to be investigated. For these simulations, the time evolution of the A-B solution was performed at $T = 700^{\circ}$, 800°, and $1000\,^{\circ}$C.

For both types of simulations, with asymmetrical phase diagram without diffusion asymmetry, and with asymmetrical phase diagram as well as diffusion asymmetry, we used the same time unit (Monte Carlo cycle, MCC) as defined in Ref. 10, corresponding to a single cycle in which a new position has been proposed to every atom of the cell. The simulation cell contained the same number of atoms (~210 000 atoms) as previously for the symmetrical system case and used the same limit conditions (periodical along the directions parallel to the surface).[10] The surface of the cell corresponds to a (001) plane. The presented results were obtained using time averaging over 1000 MCC (~210 000 events per MCC).

The simulation results were analyzed in the same way as in Ref. 10, using the same definition of the volume fraction of ordered atoms (F_0). F_0 is calculated in each (001) atomic plane of the fcc lattice, from the subsurface ($p = 2$)[10] to deeper in the bulk of the simulation cell ($p \to \infty$), for each phase AB_3, AB, and A_3B. As discussed in Ref. 10, during 3D phase formation, even for a single phase, ordered domains of different orientation can appear in the bulk. Atoms located at the interface between these domains cannot exhibit perfect ordering and, thus, are not considered in the calculation of F_0. Smaller the ordered domains, larger the number of atoms located at the domains' boundaries, and smaller F_0. Considering that the smaller ordered domains contains a given atom with its twelve first neighbors (fcc lattice in our case), it can be shown that, for a given phase in a given plane if $F_0 \geqslant 0.08$, this plane then can be considered to be fully ordered according to the considered phase. In contrast, if $F_0 < 0.08$, the considered (001) plane contains nuclei of the considered phase but is not completely ordered according to the considered phase. It can contain ordered domains related to other phases, as well as non-ordered domains (random solution).

C. Reaction energy influence on reactive diffusion

In this section, we present the simulation results obtained in the case of a phase diagram with asymmetric compound energies around $C = 0.5$ (Fig. 5) but no diffusion asymmetry between A and B. Figure 7(a) presents the phase formation sequences observed at $T = 10$ K (M-KMC), either during the reaction of an A film on a B substrate (system A/B), or the reaction of a B film on an A substrate (system B/A), when the film thickness is 50, 10, and 5 atomic monolayers (ML). The existence in the sample of the three phases AB_3, AB, and A_3B is shown versus time (MCC) on the abscissa axis. For 50-ML-thick films, the phases appear simultaneously and phase dissolution is not observed. However, for 10-ML-thick films, phases are dissolved sequentially. The film-atom richest compound, which is located at the surface, is the first to vanish, being consumed by the compound AB. The compound AB then vanishes, being consumed by the substrate-atom richest compound. In the case of a 5-ML-thick film, the phase formation is sequential. The first phase to appear is the film-atom richest phase. It forms in the surface vicinity

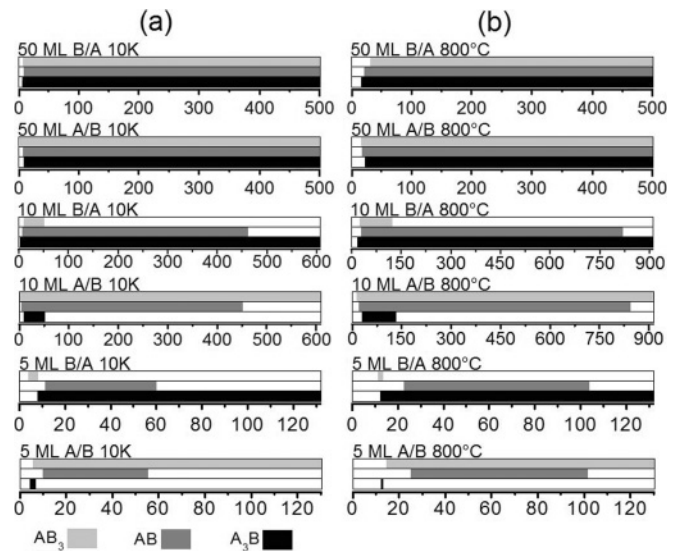

FIG. 7. Sequence of formation versus time (MCC) of the three phases A_3B (black), AB (gray), and AB_3 (light gray), for A/B and B/A systems, in the case of the dissolution of a 50-, 10-, and 5-ML-thick film at $T = 10$ K (a) and $T = 1073.15$ K (b). Simulations of a binary system exhibiting asymmetric compound energies versus composition (Fig. 5).

and vanishes quickly with the formation of the substrate-atom richest phase located deeper in the bulk of the sample (~eighth atomic plane). The phase AB forms soon after that (~5 MCC) and grows rapidly up to the surface, before being consumed by the substrate-atom richest phase. In all cases, 50-, 10-, and 5-ML-thick films for both A/B and B/A, all the phases of the A-B phase diagram are observed (Fig. 5). The phases grow or are consumed at their interfaces, and the reaction of an A film on a B substrate leads to the same sequence as for the reaction of a B film on an A substrate. All these observations are identical to the case of a totally symmetrical (reaction and diffusion) A-B system, studied in Ref. 10. The compound energy asymmetry, which involves asymmetrical compound reaction energies, has no effect on the phase formation sequence. The study of the variations of F_0 of every phase versus time shows that phase formation is sequential for a 5-ML-thick film for the same reason as for the symmetrical case: An asymmetrical interdiffusion profile forms between the film and the substrate, due to a size effect between the thicknesses of the film (Fick diffusion in a finite layer) and the substrate (Fick diffusion in a semi-infinite medium). However, one can note that, in contrast with the symmetrical case,[10] for 10- and 5-ML-thick films, the phase sequence kinetic is slightly different for the A/B and B/A cases. The lifetime of phases is longer for the reaction of a B film on an A substrate. This difference is very small for the 10-ML-thick films but is more obvious for the 5-ML-thick films, as the lifetime of the first phase to form is about 3 times longer in the B/A case. This can be explained considering that, in all cases, the thermodynamic equilibrium corresponds to the total dissolution of the atoms contained in the film. However, for the A/B case, phase stability increases with the dissolution process, since A_3B is less stable than AB, which is less stable than AB_3 (Fig. 5), while for the B/A case it is the opposite. Consequently, the

dissolution process is slightly faster for A/B than for B/A. In summary, atomistic simulations confirm that equilibrium bulk parameters, as bulk phase energies, have no effect on the phase formation sequence, as well as on the selection of the first phase to nucleate (in our case the AB_3 formation energy is about twice as large as the A_3B one; see Fig. 5). Furthermore, as the phase reaction energy is usually considered to be directly proportional to the phase formation energy, these simulations show that reaction is not the parameter controlling the sequential phase formation process. Phases nucleate in a concentration gradient, when locally, the concentration is close to their stoichiometry.[10] The degree of stability of the phase at its stoichiometry concentration is not the main issue, since even if the phase formation energy is small, the phase will tend to form in a concentration close to its stoichiometry. Consequently, the conditions allowing for the formation of a solution at the correct concentration for the phase to form seem to be the main issue.

In order to understand how these results could be modified by temperature, and to be able to compare these results with the case of asymmetric diffusion, we have also performed calculations using our S-KMC algorithm at $T = 800\ ^\circ$C, imposing a constant diffusion barrier $\Delta E = \Delta E_B$ and a constant frequency $\nu = \nu_B$ [Eq. (11)]. As can be seen in Fig. 7(b), all the conclusions driven above remain valid at high temperature, and, in particular, the fact that compound bulk energies have very weak effect on the phase sequence during sequential phase formation.

D. Atomic jump frequency influence on reactive diffusion

In this section, we present the simulation results concerning an A-B system exhibiting both an asymmetrical phase diagram (Fig. 5) and asymmetrical self-diffusivities between A and B (Fig. 6). Figure 8 presents the existence of the phases A_3B, AB, and AB_3 versus annealing time (MCC) during the reaction of a 50-, 10-, or 5-ML-thick film at two temperatures around that used for the symmetrical case (S-KMC), namely $T = 700\ ^\circ$C [Fig. 8(a)] and $T = 1000\ ^\circ$C [Fig. 8(b)]. In contrast with the previous cases (symmetrical or asymmetrical phase energy only), the phases form sequentially. The diffusion asymmetry increases the critical thickness of the simultaneous-to-sequential phase formation transition. For a 50-nm-thick film, the phase sequence is identical for A/B and B/A at the same temperature. However, the phase sequence varies with temperature. At 1000 °C, the first phase to form is A_3B. Its formation is as fast as it disappearance, which corresponds to the transient behavior. The next phase to form is AB_3 and then AB. These two last compounds coexist during ∼200 MCC before A_3B forms again. At that stage, all three phases of the A-B phase diagram coexist in the sample bulk. At 1000 °C, the phase formation sequence can be summarized as $AB_3 \rightarrow AB_3 + AB \rightarrow AB_3 + AB + A_3B$. At 700 °C, A_3B and AB_3 appear quasisimultaneously. Then, after ∼200 MCC, the phase AB forms, and the three phases coexist in the sample bulk until A_3B vanishes. The sequence at 700 °C is $A_3B + AB_3 \rightarrow A_3B + AB_3 + AB \rightarrow AB_3 + AB$. Temperature influences atomic transport kinetics, but, additionally, in our case, a temperature change involves a modification of the diffusion asymmetry between A and B atoms. When temperature

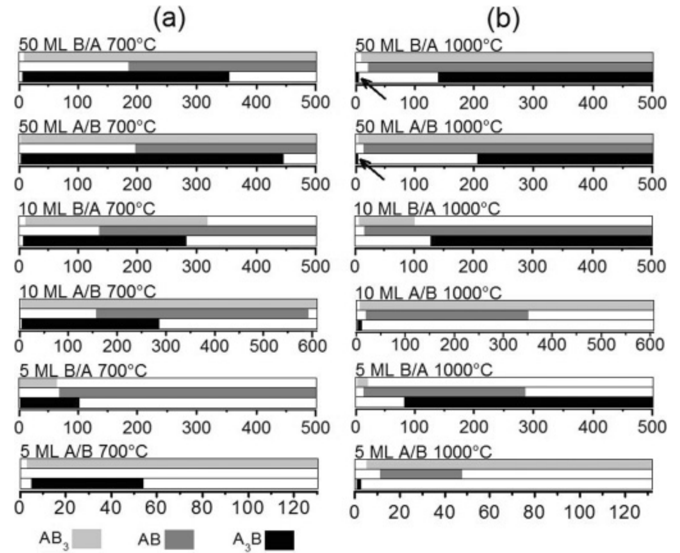

FIG. 8. Sequence of formation versus time (MCC) of the three phases A_3B (black), AB (gray), and AB_3 (light gray), for A/B and B/A systems, in the case of the dissolution of a 50-, 10-, and, 5-ML-thick film at $T = 700\ ^\circ$C (a) and $T = 1000\ ^\circ$C (b). The arrows highlight the first appearance of the A_3B phase. Simulations of a binary system exhibiting asymmetric compound energies versus composition (Fig. 5), as well as asymmetric diffusion between A and B (Fig. 6).

decreases, the diffusion asymmetry increases. At 1000 °C the ratio between B and A self-diffusion is $\sim 10^2$, while this ratio is $\sim 10^4$ at 700 °C (Fig. 6). Consequently, the simulations show that diffusion asymmetry changes the critical thickness of the simultaneous-to-sequential phase formation transition, and a change of the asymmetry level can modify the phase sequence. Furthermore, the thicknesses of the compound layers are not symmetric for A/B and B/A. The A_3B layer is always the thinnest. In addition, at 700 °C, A_3B forms simultaneously with AB_3, but the A_3B layer does not grow during the growth of the AB_3 layer. The moment A_3B is formed, its layer thickness is ∼3 ML and it does not change with time. However, the A_3B layer position shifts in the bulk of the sample, remaining at the interface with the pure A layer during the growth of AB_3 and AB. Even for the thickest films (50 ML), for which all the phases of the phase diagram can coexist in the sample bulk, a diffusion asymmetry influences the order of the phase formation and generates transient phase formation, with the appearance of a same phase several times in the sequence.

For a 10-ML-thick film, in contrast with the symmetrical case (and with a binary system with asymmetric phase energies), phases appear sequentially, and the phase sequences for A/B and B/A differ. At 1000 °C [Fig. 8(b)], the phase sequence is $AB_3 \rightarrow AB_3 + AB \rightarrow AB \rightarrow AB + A_3B$ for B/A while it is $A_3B \rightarrow A_3B + AB_3 \rightarrow AB_3 \rightarrow AB_3 + AB \rightarrow AB_3$ for A/B, which is the same sequence as for a symmetric system for a 5-ML-thick film (Fig. 7). However, it can be noted that in both cases the phase that forms first is always the richest in film-atoms. At 700 °C [Fig. 8(a)], the beginning of the phase formation sequence is similar to the sequence observed for a 50-ML-thick film. For B/A the sequence is $A_3B + AB_3 \rightarrow A_3B + AB_3 + AB \rightarrow AB_3 + AB \rightarrow AB$.

For A/B the sequence beginning is the same, but the last phase is AB_3 (the richest in substrate-atoms) instead of AB, with $A_3B + AB_3 \rightarrow A_3B + AB_3 + AB \rightarrow AB_3 + AB \rightarrow AB_3$. Similarly to the case of a 50-ML-thick film, a change in the diffusion asymmetry level leads to a modification of the phase formation sequence. For example, for B/A, the last phase to form at 1000 °C is the first phase to form at 700 °C. We can also note that the thicknesses and the lifetimes of the phases depend on the diffusion asymmetry level. For example, for B/A, the AB_3 layer is thicker at 700 °C compared to 1000 °C, while it is the opposite for the A_3B layer. For A/B, the lifetime of A_3B is shorter at 1000 °C than at 700 °C (Fig. 8). Similarly to the case of a 50-ML-thick film, when the diffusion asymmetry increases, the richest phase in A atoms exists only as a very thin layer that does not grow, localized between the pure A layer (lower diffusivity) and the other phases.

For the reaction of a 5-ML-thick film of B atoms on a A substrate, phases appear sequentially, and the phase sequences at 1000° and 700 °C are identical to the sequences observed for a 10-ML-thick film. Consequently, the same conclusions can be made for the 10- and 5-ML-thick films: The diffusion asymmetry influences the order of phase appearance, as well as the lifetimes and the thicknesses of the phases. For the reaction of a 5-ML-thick film of A atoms on a B substrate, the phase formation sequence is identical to that of a 10-ML-thick film in same conditions at 1000 °C. However, at 700 °C, the phase sequence differs, especially since the phase AB does not form. AB_3 appears slightly before A_3B. Then, during the growth of the AB_3 layer, the A_3B layer stays at the A/AB_3 interface without growing. Subsequently, A_3B vanishes and AB_3 becomes the only phase present in the sample. The sequence is $AB_3 \rightarrow AB_3 + A_3B \rightarrow AB_3$. These results show that an increase of the diffusion asymmetry can change the first phase in the sequence (A_3B at 1000 °C and AB_3 at 700 °C) and can prevent some phases (AB at 700 °C) from forming. In addition, for the same binary system A-B, in same conditions, the phase sequences are different for A/B and B/A. One can note that the phase AB is missing in the phase sequence only for the case A/B and not for the case B/A. This phase is missing when the film-atoms diffuse faster in the substrate than the substrate-atoms in the film.

The simulations show that a diffusion asymmetry can lead to different phase formation sequences between A/B and B/A and that an increase of diffusion asymmetry (which is temperature dependent) can modify the phase sequence and its kinetics. In addition, a diffusion asymmetry can promote the formation of a phase as a thin layer with constant thickness, remaining at the interface between the layer exhibiting the lowest diffusivity and the other phases. It can also promote the transient formation of some phases and prevent others from forming (missing phases).

In order to understand the mechanisms driving these phenomena, one can investigate the variation of the fraction of ordered atoms for every phase in comparison to composition variations versus depth in the sample, at different annealing times. For example, Figs. 9 and 10 show the variations of the fraction F_0 (left axis) of each phase, as well as the concentration variations of A atoms versus depth, for different annealing times during the reaction of a 10-ML-thick film at 1000 °C, in the cases A/B and B/A. Figure 9 corresponds to the formation of the first phase in the sequences (A_3B for A/B and AB_3 for B/A), and Fig. 10 corresponds to the formation of AB. These figures allow the role of the diffusion asymmetry on the difference of phase formation sequences between A/B and B/A to be understood. In both cases A/B and B/A, the first phase to appear ($F_0 \geqslant 0.08$) is the richest in film-atoms (Fig. 9). However, because of the diffusion asymmetry, the interdiffusion profile is not symmetric. This profile is abrupt on the A side and exhibits a penetration tail on the B side. For this reason, the first phases to appear for A/B and B/A exhibit different behaviors. For A/B [Fig. 9(a)], A_3B forms in the strongest composition gradient close to the pure A layer. It appears quite early (~8 MCC), but its thickness is thin, and

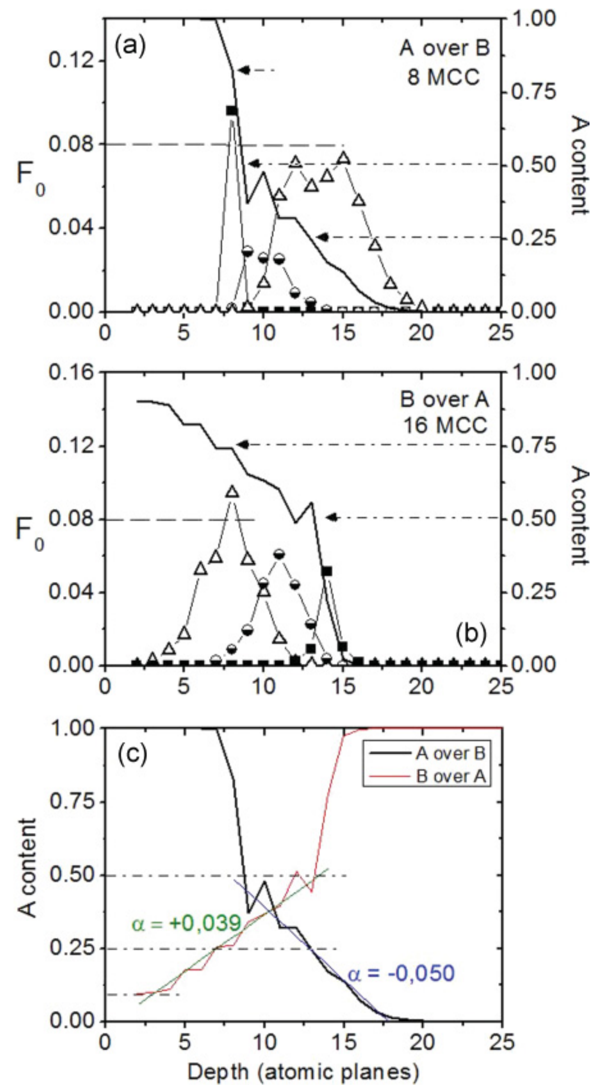

FIG. 9. (Color online) Volume fraction F_0 (left axis) of the three ordered phases A_3B (solid squares), AB (semi-solid circles), and AB_3 (open triangles), and concentration profile of A atoms (solid line, right axis) versus depth (atomic plane number, bottom axis) in the case of the dissolution of a 10-ML-thick film on a semi-infinite substrate at 1000 °C: (a) A/B at t = 8 MCC and (b) B/A at t = 16 MCC. (c) Comparison between concentration profiles presented in (a) and (b). Simulations of a binary system exhibiting asymmetric compound energies versus composition (Fig. 5), as well as asymmetric diffusion between A and B (Fig. 6).

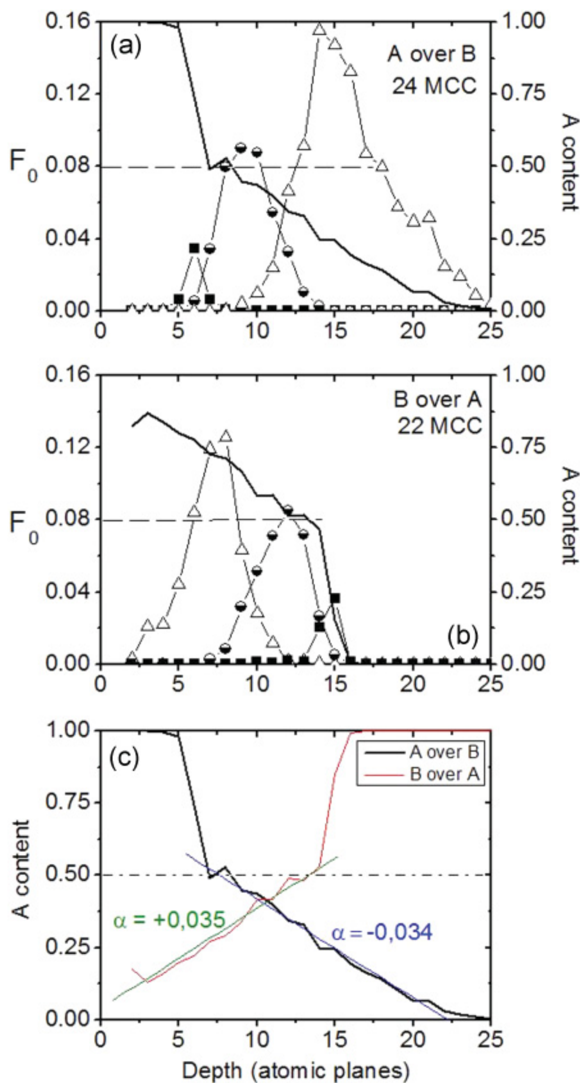

FIG. 10. (Color online) Volume fraction F_0 (left axis) of the three ordered phases A_3B (solid squares), AB (semi-solid circles), and AB_3 (open triangles), and concentration profile of A atoms (solid line, right axis) versus depth (atomic plane number, bottom axis) in the case of the dissolution of a 10-ML-thick film on a semi-infinite substrate at 1000 °C: (a) A/B at $t = 24$ MCC and (b) B/A at $t = 22$ MCC. (c) Comparison between concentration profiles presented in (a) and (b). Simulations of a binary system exhibiting asymmetric compound energies versus composition (Fig. 5), as well as asymmetric diffusion between A and B (Fig. 6).

its lifetime is short due to the variation of the interdiffusion profile close to A. For B/A [Fig. 9(b)], AB_3 forms in the composition gradient close to the pure B layer, which is less abrupt. It appears a little later (∼16 MCC) since it necessitates the formation of a diffusion tail in the B layer. However, because of the shape of this diffusion profile, it can grow thicker, and, consequently, its lifetime is longer. One can note in Fig. 9(c) that the formation of the first phase A_3B for A/B only results from the diffusion asymmetry, since $C = 1$ at the surface on the A side when this phase appears. In contrast, for B/A, the formation of the first phase AB_3 results from both the size effect between the film (finite) and the substrate (semi-infinite),[10] and the diffusion asymmetry between A and B as $C \sim 0.1$ at the surface on the B side when this phase appears. Whatever the system, A/B or B/A, a given phase always appears in a given concentration gradient, which is compatible to the stoichiometry of the phase. For example, AB_3 forms for $C \sim 0.25$ in a composition gradient exhibiting a slope $\alpha \sim \pm 0.04$ [Fig. 9(c)], while AB forms for $C \sim 0.5$ with $\alpha \sim \pm 0.035$ [Fig. 10(c)]. In the case A/B, due to the abrupt shape of the concentration profile on the A side (slow diffusion), and despite the fact that A_3B formed on the A-side, the second phase AB_3 forms in the diffusion tail on the B side [open triangles in Fig. 9(a)] with $\alpha \sim -0.04$ [Fig. 9(c)]. In contrast, for B/A, after the formation of AB_3 in the diffusion tail on the B side (fast diffusion) when $\alpha \sim +0.04$, the second phase AB also forms in the diffusion tail on the B side when $\alpha \sim +0.035$ [semisolid circles in Fig. 10(b)]. Later on, the third phase A_3B forms also in the diffusion tail on the B side once the composition gradient has decreased. In the case A/B, AB is the third phase to form [Fig. 10(a)]. Similarly to the case B/A, it appears after AB_3 ($\alpha \sim \pm 0.04$), as the composition gradient decreases until $\alpha \sim \pm 0.035$. The phase sequence can be shown to be the same for a thinner 5-ML-thick film of A atoms on a B substrate at the same temperature. The first phase A_3B forms quickly (∼2 MCC), and as it appears, the diffusion tail in the B side does not allow the formation of the second phase AB_3. Then, A_3B vanishes rapidly, and after 30 MCC AB and AB_3 coexist already. AB disappears after 60 MCC.

Repeating the calculations for a thicker 50-ML-thick B film on an A substrate at the same temperature, allows us to understand the first transient formation of A_3B and its second appearance in the phase sequence. At the beginning of the reaction, the compound A_3B that is the richest in A atoms (stable for $0.35 < C_B < 0.15$ in the phase diagram) forms on the most-abrupt side of the interdiffusion profile where $C_B \sim 0.15$. Then, as C_B decreases rapidly to zero at this location of the composition gradient (A side), A_3B vanishes rapidly. The first appearance of A_3B is transient because, at this stage of the reaction, A_3B forms in the interdiffusion profile where the composition gradient increases with time due to the diffusion asymmetry between A and B atoms. After that, the composition gradient is very abrupt on the A side, and, thus, all the following phases form in the diffusion tail on the B side, as the composition gradient decreases with time in this region of the interdiffusion profile. AB_3 forms after 13 MCC where $C_B \sim 0.75$, and then AB forms where $C_B \sim 0.5$. Later ($t = 150$ MCC), when the composition gradient in this region reaches a lower value close to $C_B \sim 0.25$, A_3B again forms and grows in this side of the interdiffusion profile. In contrast with its first appearance, for the second, A_3B forms in the least-abrupt part of the interdiffusion profile, where the composition gradient decreases with time. This is why, at that time, A_3B can grow and its lifetime is significantly longer.

Finally, to understand why a phase can be missing in the phase formation sequence, and why a phase can exist as a thin layer of constant thickness, Fig. 11 presents the variations of F_0 of each phase, as well as the concentration profile of A atoms versus depth at different reaction times corresponding to the reaction of a 5-ML-thick film of A atoms on a B substrate at 700 °C. After 7 MCC, the phases A_3B and AB_3 already coexist in the sample. A_3B is located on the most-abrupt side of the interdiffusion profile, the richest in A atoms, while AB_3 is

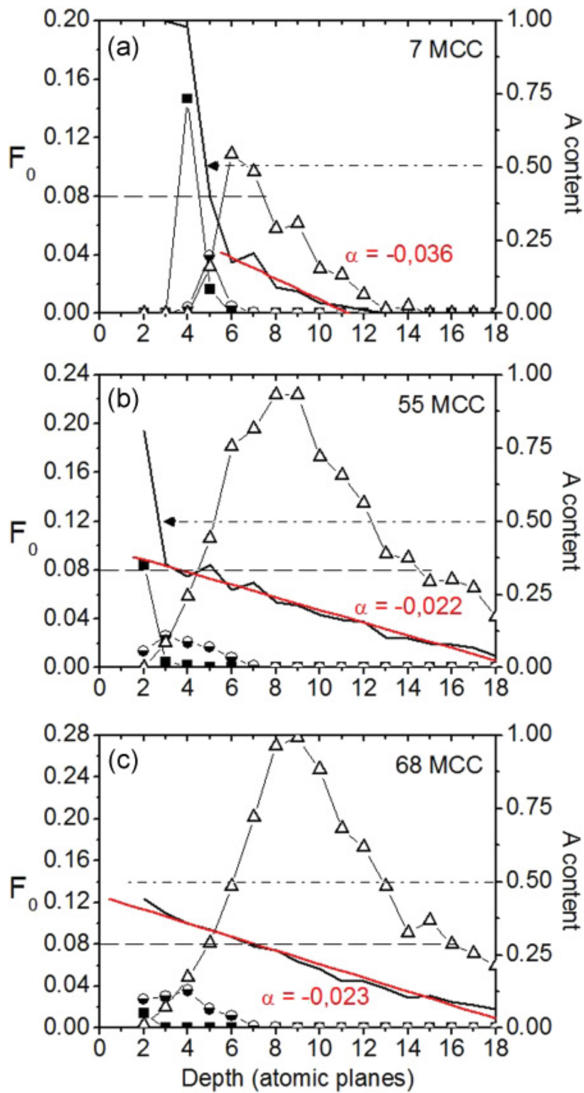

FIG. 11. (Color online) Volume fraction F_0 (left axis) of the three ordered phases A_3B (solid squares), AB (semi-solid circles), and AB_3 (open triangles), and concentration profile of A atoms (solid line, right axis) versus depth (atomic plane number, bottom axis) in the case of the dissolution of a 5-ML-thick film of A atoms on B substrate at 700 °C: (a) $t = 7$ MCC, (b) $t = 55$ MCC, and (c) $t = 68$ MCC. Simulations of a binary system exhibiting asymmetric compound energies versus composition (Fig. 5), as well as asymmetric diffusion between A and B (Fig. 6).

located on the least-abrupt side of the interdiffusion profile, the richest in B atoms. Because of the weak penetration of B atoms in A, and of the strong penetration of A atoms in B, the A_3B layer is very thin, while the AB_3 layer is thicker [Fig. 11(a)]. One can note in Fig. 11(a) that at this moment the concentration gradient around $C = 0.5$ is too abrupt to allow the formation of AB. Later, during the reaction, the shape of the interdiffusion profile stays almost the same, but it is shifting toward the film A, which is consumed almost atomic plane per atomic plane [Fig. 11(b)]. Thus, the A_3B layer cannot grow, but it is shifted toward the film of A atoms, following the interdiffusion profile, while the AB_3 layer is growing with the consumption of the A film. For example, after 55 MCC [Fig. 11(b)], the A_3B layer is shifted two atomic planes without growing (it is centered on plane 4 at 7 MCC, and on plane 2 at 55 MCC), and the AB_3 layer thickness increased by eight atomic planes. One can note that, at this moment, AB is still not formed because of the abruptness of the interdiffusion profile around $C = 0.5$. Because of the strong diffusion asymmetry between A and B at 700 °C, this plane-by-plane dissolution process of the film is maintained until the surface plane is reached. Thus, when the last atomic planes of the A film are dissolved, the concentration of these planes changes rapidly from a concentration significantly higher than $C = 0.5$ [Fig. 11(b)] to a concentration significantly lower than $C = 0.5$ with a low concentration gradient [$\alpha \sim -0.023$, Fig. 11(c)]. This process is shown in Fig. 11(c) for $t = 68$ MCC. Because of this phenomenon, during the whole reaction, the concentration gradient between A and B can never support the formation of AB. Once A_3B has vanished, only AB_3 is present in the sample, and only this phase can grow in the composition gradient existing in the sample. The phase AB is missing in the phase formation sequence. The shift of the thin A_3B layer without growth is explained by the very small diffusion of B atoms in pure A and the plane-by-plane reaction of the film. The simulations show that the thickness of the compound layers is inversely proportional to the concentration gradient existing in the sample around their stoichiometry concentration and proportional to their composition range of stability in the phase diagram.

E. Comparison with experimental results

Experimental studies[7,30,31] show that when an Ni film of tens of nanometers reacts with an Si substrate (system Ni/Si), the phase Ni_3Si does not usually appear in the sequence, and the phases $Ni_{31}Si_{12}$ and Ni_3Si_2 exhibit a transient formation. However, recent experiments[32] showed that during the reaction of a 5-ML-thick Si film on Ni (system Si/Ni), all the Si-Ni phases seem to appear one after the other during sequential formation. In the case of Ni/Si, in some experiments, especially when a small concentration of Pt atoms (∼5%) is dissolved in the Ni film,[33,34] the formation of a thin NiSi layer (5–9 nm) was observed at the interface between Si and the other phases from the beginning of the reaction. Furthermore, this layer was shown to not grow until all the phases of the sequence have been consumed. These phenomena cannot be reproduced by a symmetric system, nor by a system exhibiting asymmetric compound formation energies versus composition. In contrast, when the system exhibits a diffusion asymmetry, phenomena close to the experimental observations can be simulated: (i) A given phase existing in the phase diagram can be missing in the phase formation sequence, similarly to the case of Ni_3Si, due to a very abrupt interdiffusion profile; (ii) a given phase can exhibit a transient formation, similarly to $Ni_{31}Si_{12}$ and Ni_3Si_2, if it forms on the most-abrupt side of the interdiffusion profile, where the concentration profile changes faster since atoms in this region can diffuse faster in the rest of the sample; (iii) similarly to the experimental system Si-Ni, the phase formation sequences for Ni/Si and Si/Ni differ due to the interdiffusion profile asymmetry; and (iv) a phase that forms in the abrupt part of the interdiffusion profile can exhibit a constant thickness, rather thin, due to the local shape of the interdiffusion profile or due to the plane-by-plane dissolution

of the phase with which it is in contact, as observed in the case of the thin NiSi film in contact with Si when Pt is present in Ni. In the simulations, transient phase formation and missing phases are observed in the case A/B. This corresponds to the case for which the atoms of the film diffuse faster in the substrate than the atoms of the substrate in the film. In the experiment, this corresponds to the case Ni/Si. Indeed, the diffusivities of A and B atoms were chosen to correspond to the self-diffusivities of Si and Ni, respectively, but it has been experimentally shown that during the formation of Si-Ni compounds, the diffusivity of Si atoms can be neglected compared to the diffusivity of Ni atoms. Our simulations rather correspond to the case where A and B atoms both use the vacancy mechanism to diffuse in all the phases, which is more in agreement with a diffusion coefficient proportional to the matrix composition. However, the experimental Si-Ni system is more complex since Ni diffusion in Si does not use the same mechanism as Si diffusion in Ni. Ni diffuses in Si using the interstitial mechanism, while Si is supposed to diffuse in Ni via vacancies. Thus, the diffusion asymmetry in the experimental Si-Ni system corresponds to the reverse case in simulations. The case A/B in the simulations corresponds to the case Ni/Si in the experiment. The simulation results are, thus, in agreement with the experimental observations: They predict that during the reaction of an Si film on an Ni substrate, all the phase of the phase diagram should appear during sequential formation,[32] while during the reaction of an Ni film on an Si substrate, Ni-rich phases could exhibit a transient behavior, and others could be missing.[7,30,31] However, the thin film exhibiting a constant thickness during reaction is in contact with A in the simulations (region of low diffusivity for B atoms), whereas the thin NiSi layer is in contact with Si in the experiments (region of high diffusivity for Ni atoms). This difference may be due to more complex diffusion properties of real Si-Ni compounds. Indeed, in the simulation, the diffusion parameters [Eqs. (12) and (13)] vary linearly with composition. However, the diffusion in the Si-Ni compounds may be more complex as these compounds exhibit different crystalline structures, in addition to different compositions. The diffusion of atoms may vary significantly from one phase to another since the atomic diffusion mechanisms can differ from phase to phase. For example, the diffusion coefficients of As[35] and B[36,37] were shown to exhibit large variations in Ni_2Si and NiSi in grains, as well as in GBs. In addition, stress effects on atomic diffusion[30,38–41] were not taken into account in our simulations. For example, stress relaxation during reaction may lead to time-dependent diffusion coefficients.

IV. CONCLUSION

Influences of reaction and diffusion kinetics on reactive diffusion were investigated using atomistic KMC simulations, considering the thermodynamic model of the nonregular solid solution on a rigid fcc lattice, in the case of a binary system composed of two types of generic atoms A and B. The simulations show that compound bulk energy variations (i.e., reaction rate variations) have no effect on the phase sequence during sequential phase formation. However, compound bulk energy can influence the kinetics of the phase sequence due to the relative stability of the compounds appearing sequentially (dissolution from A-rich compounds to B-rich compounds or vice versa). Despite the important compound energy asymmetry of our system versus composition, the same sequence is observed for the reaction of an A film on a B substrate, or a B film on an A substrate, and the same phase sequence is observed as for a symmetric solution. In contrast, a diffusion asymmetry between A and B atoms has a significant impact on the interdiffusion profile and, thus, on the phase sequence. It increases the critical thickness of the simultaneous-to-sequential phase formation transition and modifies the order of phases in the formation sequence. In particular, it has a significant influence on the selection of the first phase appearing in the sequence. Due to diffusion asymmetry, the phase sequences are not the same for A/B and B/A systems, and transient phase formation can be observed. Furthermore, a diffusion asymmetry can prevent some phases of the phase diagram from appearing during sequential formation. The simulations also show that the diffusion asymmetry influences the phase thicknesses and their lifetimes during reactive diffusion. The atomistic simulations show that during reactive diffusion, sequential phase formation does not result from a competition between diffusion and reaction, as proposed by macroscopic models. Sequential phase formation results from the formation of an asymmetric interdiffusion profile due to either a size effect between film and substrate or a diffusion competition between the different elements of the system in the bulk of the different compounds. Consequently, the simulations predict that the phase formation sequence of a given binary system can be changed by modifying atom diffusivities, for example, thanks to the introduction of impurities.

ACKNOWLEDGMENTS

The authors thank K. Hoummada for interesting discussions, as well as M. Portavoce for proofreading the article.

*alain.portavoce@im2np.fr

[1] R. C. Reed, *The Superalloys: Fundamentals and Applications* (Cambridge University Press, New York, 2006), p. 283.

[2] S. M. Sze, *VLSI Technology* (International Edition, Singapore, 1988), p. 397.

[3] U. Gösele and K. N. Tu, J. Appl. Phys. **53**, 3252 (1982).

[4] F. M. d'Heurle and P. Gas, J. Mater. Res. **1**, 205 (1986).

[5] K.-N. Tu, J. W. Mayer, and L. C. Feldman, *Electronic Thin Film Science for Electrical Engineers and Materials Scientists* (Macmillan Publishing Company, New York, 1992) p. 302.

[6] S.-L. Zhang and F. M. d'Heurle, Mater. Sci. Forum **155-156**, 59 (1994).

[7] F. Nemouchi, D. Mangelinck, C. Bergman, and P. Gas, Appl. Phys. Lett. **86**, 041903 (2005).

[8] S. U. Campisano, G. Foti, E. Rimini, S. S. Lau, and J. W. Mayer, Philos. Mag. **31**, 903 (1975).

[9] E. Philofsky, Solid State Electronics **13**, 1391 (1970).

[10] A. Portavoce and G. Tréglia, Phys. Rev. B **82**, 205431 (2010).

[11] C. Lavoie, F. M. d'Heurle, C. Detavernier, and C. Cabral, Microelectron. Eng. **70**, 144 (2003).

[12]O. Chaix-Pluchery, B. Chenevier, I. Matko, J. P. Sénateur, and F. La Via, J. Appl. Phys. **96**, 361 (2004).
[13]G. L. Katona, Z. Erdélyi, D. L. Beke, C. Dietrich, F. Weigl, H.-G. Boyen, B. Koslowski, and P. Ziemann, Phys. Rev. B **71**, 115432 (2005).
[14]Z. Balogh, Z. Erdélyi, D. L. Beke, G. A. Langer, A. Csik, H.-G. Boyen, U. Wiedwald, P. Ziemann, A. Portavoce, and C. Girardeaux, Appl. Phys. Lett. **92**, 143104 (2008).
[15]Z. Erdélyi, Z. Balogh, and D. L. Beke, Acta Mater. **58**, 5639 (2010).
[16]G. Tréglia, B. Legrand, and F. Ducastelle, Europhys. Lett. **7**, 575 (1988).
[17]A. Senhaji, G. Tréglia, B. Legrand, N. T. Barrett, C. Guillot, and B. Villette, Surf. Sci. **274**, 297 (1992).
[18]A. Senhaji, G. Tréglia, J. Eugène, A. Khoutami, and B. Legrand, Surf. Sci. **287**/**288**, 371 (1993).
[19]F. Ducastelle, *Order and Phase Stability in Alloys -Cohesion and Structure Vol. 3-* (North-Holland/Elsevier, Amsterdam, 1991).
[20]Z. Erdélyi, D. L. Beke, and A. Taranovskyy, Appl. Phys. Lett. **92**, 133110 (2008).
[21]A. Bieber, F. Gautier, G. Tréglia, and F. Ducastelle, Solid State Commun. **39**, 149 (1981).
[22]O. Kubaschewski and J. A. Catterall, *Thermochemical Data of Alloys* (Pergamon Press, New York, 1956), p. 55.
[23]F. R. de Boer, R. Boom, W. C. M. Mattens, A. R. Miedema, and A. K. Niessen, *Cohesion in Metals: Transition Metal Alloys* (Elsevier, Amsterdam, 1988), p. 293.
[24]C. Kittel, *Introduction to Solid State Physics* (John Wiley & Sons, New York, 2005), p. 47.
[25]N. Metropolis, A. W. Metropolis, M. N. Rosenbluth, A. H. Teller, and E. Teller, J. Chem. Phys. **21**, 1087 (1953).
[26]A. B. Vladimirov, V. N. Kaigorodov, S. M. Klotsman, and I. S. Tracktenberg, DIMETA **82**, *Proc. Int. Conf. on Diffusion in Metals and Alloys, Tihany, 1982*, edited by F. J. Kedves and D. L. Beke (Trans. Tech. Publication, Switzerland, 1983), p. 338.
[27]P. Pichler, *Intrinsic Point Defects, Impurities, and Their Diffusion in Silicon* (Springer-Verlag, Wien, Austria, 2004), p. 92.
[28]S. Z. Bokshtein, S. T. Kishkin, Y. M. Mishin, and I. M. Razumovskii, Dokl. Akad. Nauk SSSR **280**, 1125 (1985).
[29]A. Portavoce, G. Chai, L. Chow, and J. Bernardini, J. Appl. Phys. **104**, 104910 (2008).
[30]C. Rivero, P. Gergaud, M. Gailhanou, O. Thomas, B. Froment, H. Jaouen, and V. Carron, Appl. Phys. Lett. **87**, 041904 (2005).
[31]J. A. Kittl, M. A. Pawlak, C. Torregiani, A. Lauwers, C. Demeurisse, C. Vrancken, P. P. Absil, S. Biesemans, C. Coia, C. Detavernier, J. Jordan-Sweet, and C. Lavoie, J. Appl. Phys. **91**, 172108 (2007).
[32]A. Portavoce, B. Lalmi, G. Tréglia, C. Girardeaux, D. Mangelinck, B. Aufray, and J. Bernardini, Appl. Phys. Lett. **95**, 023111 (2009).
[33]C. Lavoie, C. Coia, F. M. d'Heurle, C. Detavernier, C. Cabral, P. Desjardins, and A J. Kellock, Defect Diffus. Forum **237**, 825 (2005).
[34]K. Hoummada, C. Perrin-Pellegrino, and D. Mangelinck, J. Appl. Phys. **106**, 063511 (2009).
[35]I. Blum, A. Portavoce, D. Mangelinck, R. Daineche, K. Hoummada, J. L. Lábár, V. Carron, and C. Perrin, J. Appl. Phys. **104**, 114312 (2008).
[36]I. Blum, A. Portavoce, L. Chow, D. Mangelinck, K. Hoummada, G. Tellouche, and V. Carron, Appl. Phys. Lett. **96**, 054102 (2010).
[37]A. Portavoce, I. Blum, D. Mangelinck, K. Hoummada, L. Chow, V. Carron, and J. L. Lábár, Scr. Mater. **64**, 828 (2011).
[38]A. Portavoce, P. Gas, I. Berbezier, A. Ronda, J. S. Christensen, A. Yu. Kuznetsov, and B. G. Svensson, Phys. Rev. B **69**, 155415 (2004).
[39]A. Portavoce, P. Gas, I. Berbezier, A. Ronda, J. S. Christensen, and B. Svensson, J. Appl. Phys. **96**, 3158 (2004).
[40]D. Mangelinck and K. Hoummada, Appl. Phys. Lett. **92**, 254101 (2008).
[41]C. Van Bockstael, K. De Keyser, D. Deduytsche, R. L. Van Meirhaeghe, C. Detavernier, J. L. Jordan-Sweet, and C. Lavoie, J. Appl. Phys. **104**, 053510 (2008).